Neuron, Vol. 33, 893–903, March 14, 2002, Copyright ©2002 by Cell Press

Novel Modulation of Neuronal Nicotinic Acetylcholine Receptors by Association with the Endogenous Prototoxin lynx1

Inés Ibañez-Tallon,[1] Julie M. Miwa,[1] Hai-Long Wang,[3] Niels C. Adams,[2] Gregg W. Crabtree,[4] Steven M. Sine,[3] and Nathaniel Heintz[1,5]

[1]Laboratory of Molecular Biology
Howard Hughes Medical Institute
[2]Laboratory of Developmental Neurobiology
The Rockefeller University
New York, New York 10021
[3]Receptor Biology Laboratory
Department of Physiology and Biophysics
Mayo Foundation
Rochester, Minnesota 55905
[4]Department of Cell Biology and Anatomy
Center for Neurobiology and Behavior
Columbia University
New York, New York 10032

Summary

We previously identified lynx1 as a neuronal membrane molecule related to snake α-neurotoxins able to modulate nAChRs. Here, we show that lynx1 colocalizes with nAChRs on CNS neurons and physically associates with nAChRs. Single-channel recordings show that lynx1 promotes the largest of three current amplitudes elicited by ACh through $\alpha_4\beta_2$ nAChRs and that lynx1 enhances desensitization. Macroscopic recordings quantify the enhancement of desensitization onset by lynx1 and further show that it slows recovery from desensitization and increases the EC_{50}. These experiments establish that direct interaction of lynx1 with nAChRs can result in a novel type of functional modulation and suggest that prototoxins may play important roles in vivo by modulating functional properties of their cognate CNS receptors.

Introduction

Neuronal excitability mediated through ligand-gated neurotransmitter receptors is fine-tuned by a complex array of modulatory mechanisms. These mechanisms exist in a hierarchy of control systems from classical neuromodulators, circulating hormones, and enzymes to mechanisms that alter the conformation of the receptor such as phosphorylation, subunit composition, and assembly cofactors. Neuromodulators potentially could affect receptor function through a vast repertoire of biophysical alterations such as changes in the conductance, open time, rate of desensitization, ligand affinity, and ionic selectivity of the receptor. Alternative forms of regulation have recently come to light, such as buffering of ACh by glial secretion of a soluble Ach-binding protein, AChBP (Smit et al., 2001).

We previously reported the presence of an endogenous prototoxin, lynx1, in the mammalian CNS (Miwa et al., 1999) and showed that it alters the function of nicotinic receptors in vitro. lynx1 adopts the three-fingered toxin fold characteristic of α-neurotoxins, such as the bungarotoxins, which bind to and irreversibly inhibit nAChRs (Sine, 1997; Grant et al., 1998; Hall, 1999) and the muscarinic toxins, which selectively antagonize muscarinic AChRs (reviewed by Tsetlin, 1999). lynx1 alters the function of nicotinic receptors when applied as a soluble protein to oocytes expressing these receptors, although no direct interaction between lynx1 and nAChRs has been reported (Miwa et al., 1999). In contrast to snake toxins, which are secreted into venom, lynx1 has a consensus sequence for attachment to the cell membrane via a glycophosphatidylinositol (GPI) anchor. Since anchorage of lynx1 to the cell surface presents opportunities for novel and dynamic mechanisms of receptor modulation and regulation, we have been interested in studying the mechanisms by which lynx1 modulates nAChRs. Given the critical roles of nAChRs in complex brain function (Everitt and Robbins, 1997; Lindstrom, 1997; Changeux et al., 1998) and the observations that nAChR mutations can severely disrupt CNS function (Steinlein et al., 1995; Phillips et al. 2001), evidence for a novel modulator for the cholinergic pathway could have important physiological implications.

In this study, we use biochemical and electrophysiological approaches to establish the mechanism of action of lynx1 on nAChRs. We demonstrate that lynx1 colocalizes with nAChRs on the somatodendritic membrane of many neurons and that lynx1 can bind directly to nAChRs. Furthermore, single-channel recordings from mammalian cells expressing lynx1 and $\alpha_4\beta_2$ nAChRs reveal that lynx1 promotes the largest of three current amplitudes and enhances desensitization. Recordings of macroscopic currents in *Xenopus* oocytes quantify the acceleration of desensitization onset and further show that lynx1 slows recovery from desensitization and increases the EC_{50} for activation by ACh. These novel actions of lynx1 suggest that it and other members of this large gene family, including those expressed in the mammalian (Horie et al., 1998; our unpublished data) and invertebrate (Chou et al., 2001) nervous systems, encode a new mechanistic class of receptor modulatory proteins.

Results

Immunohistochemical Colocalization of lynx1 and Neuronal Nicotinic Receptors

lynx1 is enriched in discrete neuronal populations, similar to patterns of nAChR distribution previously reported (Hill et al., 1993; Dominguez del Toro et al., 1994; Nakayama et al., 1995; Rogers et al., 1998). We were particularly interested in establishing an in vivo association of lynx1 with nicotinic receptors. 17 nAChR subunits have been cloned from vertebrates (Lukas et al., 1999; Elgoyhen et al., 2001); five of them are expressed in skeletal muscle and the other 12 in the CNS and PNS. The most abundant subtypes in the CNS are $\alpha_4\beta_2$ and α_7

[5]Correspondence: heintz@rockefeller.edu

nAChRs (Role and Berg, 1996). We performed double-label immunofluorescence studies on mouse brain sections to determine whether lynx1 and nAChRs containing α_4 and α_7 subunits colocalize in the same neurons.

Experiments were done using both monoclonal antibodies raised against purified recombinant lynx1 protein and affinity-purified polyclonal antibodies raised against a lynx1 peptide (see Experimental Procedures). The lynx1 monoclonal antibody (mAb 8589) used in this study was chosen because it specifically stained cells transfected with a lynx1 expression vector (Figures 1A and 1B) and because immunohistochemical studies revealed a pattern of staining similar to that obtained for lynx1 by in situ hybridization (Miwa et al., 1999; data not shown). The lynx1 polyclonal antibody has been previously reported (Miwa et al., 1999). For this study, the crude antiserum was further purified on a peptide affinity column. The specificity of the purified polyclonal antibody for lynx1 was tested by comparative immunofluorescence studies on mouse brain sections (Figure 2) and Western blot (Figure 4). The results of these studies establish that both antibody preparations recognize lynx1.

To determine whether lynx1 and the nAChR α_4 subunit are colocalized on the surface of CNS neurons, double-immunoflourescence experiments were performed using the lynx1 monoclonal antibody (mAb 8589) and anti-α_4 nAChR polyclonal antibody (Rogers et al., 1998). Colocalization of lynx1 and the α_4 nAChR was evident in specific subsets of neurons in multiple regions within the CNS (Figures 1C–1F). Particularly strong labeling was detected in cerebral cortex, thalamus, substantia nigra, and cerebellum. In the telencephalon, prominent double-label immunofluorescence was detected on the membranes of the soma and apical dendrites of deep-layer cortical pyramidal cells (Figure 1C) and basolateral amygdala neurons (Figure1D). The thalamus exhibited high and widespread double immunoreactivity for lynx1 and α_4-containing receptors, including cells of the reticular and ventroposterior thalamic nucleus and habenular complex (Figure 1E). In the ventral mesencephalon, most neurons of the substantia nigra (Figure 1F) and globus pallidus (data not shown) showed specific double staining. Similar colocalization results were obtained using different secondary antibodies. No staining was detected when the primary antibodies were omitted (data not shown). Because α_4 and α_7 nAChR subunits can be coexpressed in some CNS cell types (Dominguez del Toro et al., 1994; Nakayama et al., 1995; Rogers et al., 1998), we also looked for colocalization of lynx1 and α_7 nAChRs. Double-immunofluorescence experiments of lynx1 and the nAChR α_7 subunit were performed using the affinity-purified lynx1 polyclonal antibody and the anti-α_7 nAChR monoclonal antibody mAb 306 (Schoepfer et al., 1990). lynx1 colocalizes with α_7 receptors on the surface of many neurons, including those of the cerebral cortex (Figure 2B), amygdala (Figure 2C), CA3 hippocampal neurons (Figure 2D), and reticular thalamic nucleus (Figure 2E). These results establish that lynx1 localizes to neurons expressing multiple types of nAChRs, indicating the potential of lynx1 to modulate nAChR function.

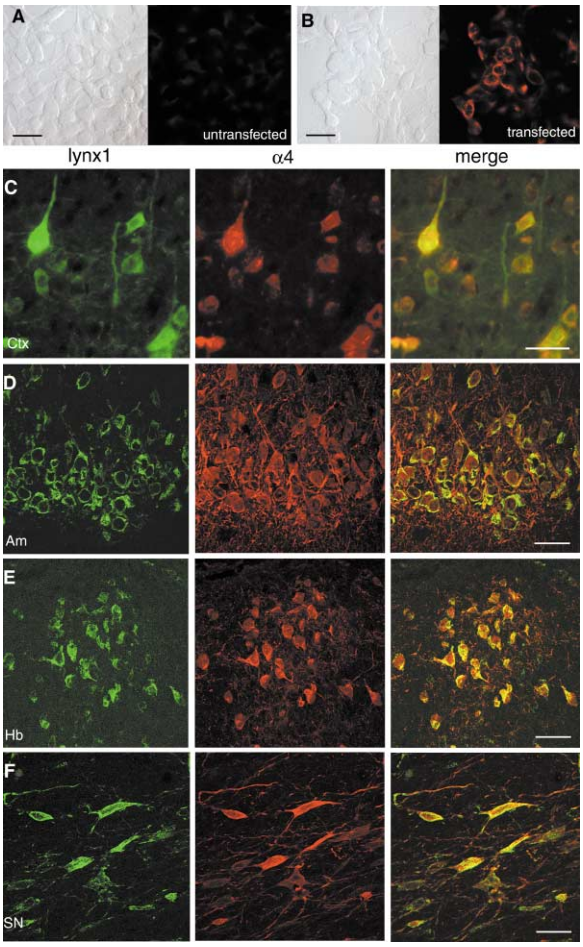

Figure 1. lynx1 Colocalizes with α_4 Nicotinic Receptors in the Somatodendritic Compartment of Several CNS Neurons

(A and B) HEK 293T cells were either untransfected (A) or transfected with a lynx1 expression vector (B), stained with the anti-lynx1 mAb 8589, and viewed with bright field (left) or with fluorescence (right) optics. Specific rim immunostaining is observed in lynx1 transfected cells.

(C–F) Distribution of lynx1 and α_4 nAChR subunit immunoreactivity in multiple regions within the CNS. Mouse brain sections were double stained with the anti-lynx1 mAb 8589 (green) and with an anti-α_4 antiserum (red). Merged images are shown in the third column. High-power confocal photomicrographs of cerebral cortex (C), amygdala (D), habenular complex (E), and substantia nigra (F) show strong double immunofluorescence in the soma and dendritic processes of distinct neurons. (C) and (F) are sagittal sections, and (D) and (E) are coronal sections.

Scale bars correspond to 12.5 μm.

lynx1 Forms a Stable Complex with Nicotinic Receptors

To determine whether lynx1 can form a stable complex with nAChRs, we performed coimmunoprecipitation experiments using HEK 293T cells expressing lynx1 and α_7 or Flag-tagged α_4 and β_2 nAChRs (Figure 3). Membrane fractions were isolated from cells transfected with only lynx1 (Figure 3A) or with lynx1 and the indicated nAChRs (Figures 3B and 3C). After detergent extraction of the Triton X-100 insoluble membrane fractions, nAChR subunits were immunoprecipitated by incubation with protein G beads bound to either α_7 (IPα_7) or α_4 (IPα_4) mono-

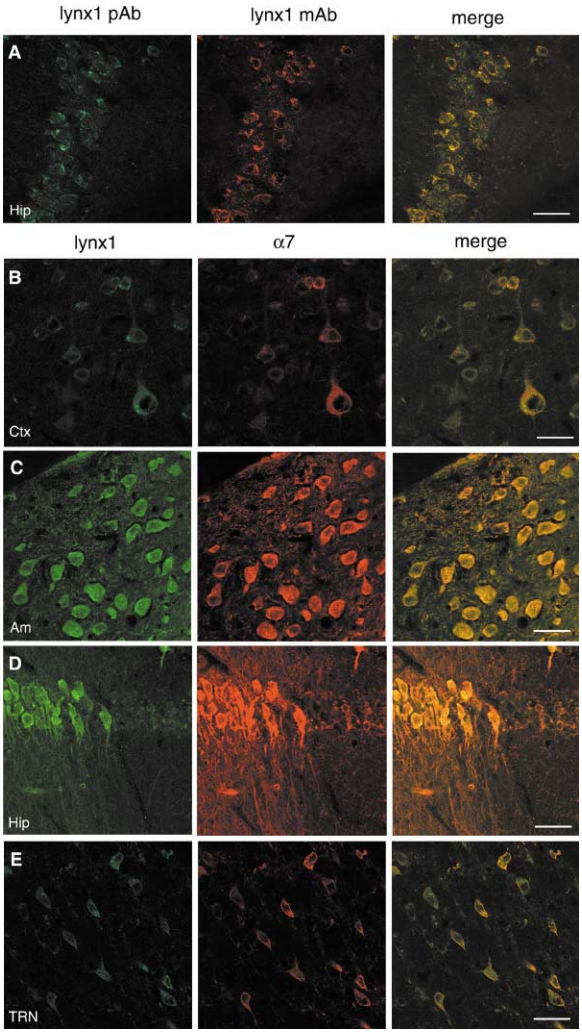

Figure 2. Specific CNS Neurons Show lynx1 and α_7 Nicotinic Receptor Double Immunoreactivity

(A) Double immunofluorescence with two lynx antibody preparations show similar labeling at the membrane. Mouse brain sections were double stained with affinity-purified anti-lynx1 polyclonal antibody (green) and anti-lynx1 mAb 8589 (red). The individual and merged confocal images of CA3 hippocampal neurons reveal immunoreactivity to both antibodies at the somatic membrane.

(B–E) Distribution of lynx1 and α_7 subunit immunoreactivity in different CNS areas. Double-staining fluorescence on mouse sagittal brain sections was done with affinity-purified anti-lynx1 polyclonal antibody (green) and with anti-α_7 mAb 306 (red). Merged images are shown on the third column. High-power confocal photomicrograph of cortical pyramidal neurons (B), cells of the amygdala (C), CA3/CA1 hippocampal neurons (D), and thalamic reticular nuclei (E) indicate marked colocalization of lynx1 and α_7 at the cell membrane of individual neurons.

Scale bars correspond to 12.5 μm.

clonal antibodies. Immunodetection with a polyclonal α_7 antibody (Figures 3A and 3B) and with an antibody against the Flag epitope (Figure 3C) showed that α_7 and $\alpha_4\beta_2$ receptors were specifically immunoprecipitated. Immunoblot analysis of the same fractions with a lynx1 polyclonal antibody (lower panels) demonstrated that lynx1 coimmunoprecipitates with both α_7 (Figure 3B) and with $\alpha_4\beta_2$ nAChRs (Figure 3C). Control experiments with extracts from cells transfected with lynx1 only (Figure 3A) demonstrated that lynx1 was not precipitated in the absence of the receptor, with protein G beads alone, or with beads carrying the α_7 monoclonal antibodies. These results demonstrate that lynx1 can form a stable complex with nAChRs in mammalian cells.

To test the specificity of lynx1 association with nicotinic receptors, we used the same immunoprecipitation protocol to look for association of lynx1 with the delta 2 glutamate receptor (Grid2). To ensure that the results of the immunoprecipitations could be directly compared, we used Flag epitope-tagged constructs for all of the receptor subunits and performed the immunoprecipitations for both the α_4 and β_2 nAChRs and Grid2 using anti-Flag antibody beads. Immunoprecipitation of extracts from cells expressing the Flag-tagged $\alpha_4\beta_2$ receptors and lynx1 or Flag-tagged Grid2 receptors and lynx1 significantly enriched both receptor types in the precipitate relative to the input fraction (Figure 3D). In contrast, lynx1 was enriched only in the precipitates from cells also expressing the $\alpha_4\beta_2$ receptors, but not in extracts from cells coexpressing the Grid2 receptors.

As an additional control for the specificity of the interaction between lynx1 and nAChRs, we tested whether these receptors could be precipitated with a second unrelated GPI-anchored protein. Immunoprecipitation of extracts from cells transfected with $\alpha_4\beta_2$ receptors and the GPI-linked protein placental alkaline phosphatase (PLAP), under conditions identical to those used to reveal the interaction of the $\alpha_4\beta_2$ nAChR and lynx1, demonstrated clear precipitation of the α_4 and β_2 subunits with the anti-Flag antibodies, as expected, but did not result in coprecipitation of PLAP (Figure 3E). This result demonstrates that the association of lynx1 and nAChRs does not result from adventitious coprecipitation due to nonspecific colocalization of nAChRs and GPI-anchored proteins in lipid rafts or other membrane subdomains. Taken together, these experiments establish that lynx1 can form specific and stable complexes with both of the major subtypes of neuronal nAChRs.

lynx1 Alters Single-Channel Currents through $\alpha_4\beta_2$ nAChRs

We previously observed that application of soluble lynx1 to α_7 and $\alpha_4\beta_2$ nAChRs increased ACh-evoked currents (Miwa et al., 1999). The immunoprecipitation data demonstrate that native GPI-anchored lynx1 is present in membrane fractions and that it can form a stable complex with nAChRs. Prompted by these results, we examined the effects of lynx1 on nAChR function when coexpressed in its native GPI-anchored form with $\alpha_4\beta_2$ receptors. To determine whether lynx alters the function of individual receptors, we carried out expression experiments in cultured mammalian cells and recorded ACh-induced single-channel currents. Using the cell-attached mode of recording and a range of ACh concentrations in the recording pipette (10–100 μM), we regularly observed single-channel currents from cells transfected with α_4 and β_2 cDNAs. However, unitary events were extremely rare when lynx1 cDNA was included in the transfection (data not shown). We reasoned that the cell-attached mode of recording allowed steady state exposure to ACh, which desensitized receptors to a

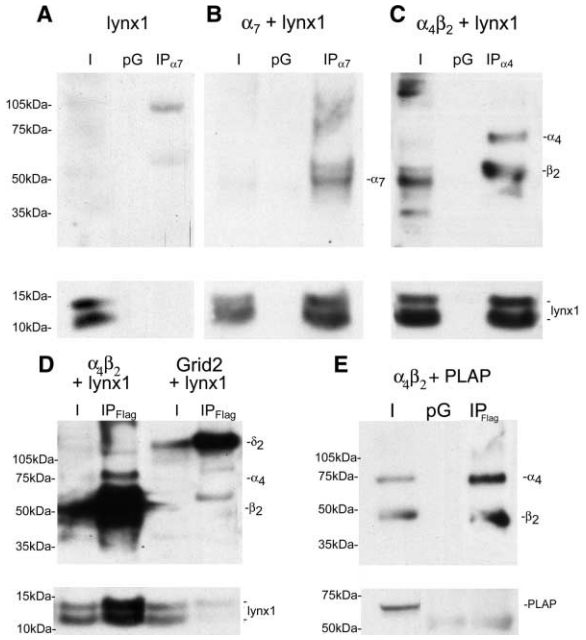

Figure 3. lynx1 Forms a Stable Complex with Nicotinic Receptors

Western blot analysis of the fractions obtained from membrane-enriched extracts prepared from HEK 293T cells transfected with either only lynx1(A), α_7 nAChR and lynx1(B), Flag-tagged α_4 and β_2 nAChR and lynx1 (C and D), Flag-tagged delta 2 glutamate receptor (Grid2) and lynx1 (D), or Flag-tagged α_4 and β_2 nAChR and GPI-linked PLAP (E) expression constructs. The first lane in each blot contains a sample of the cell extract input, indicated by the letter I. The immunoprecipitate fractions obtained by incubation of the indicated cell extracts with only protein G beads (pG) or with protein G beads coupled to the monoclonal antibodies: anti-α_7 (IPα_7), anti-α_4 (IPα_4), or anti-Flag M2 (IP$_{Flag}$) are shown in the next lanes.

(A) Western blot probed with α_7 polyclonal antibody (upper panel) does not detect any specific band. Incubation of the same blot with affinity-purified lynx1 polyclonal antibody (lower panel) reveals a doublet of bands corresponding to lynx1, migrating at ~11–13 kDa in the I fraction, and not in the pG or IPα_7 fractions, indicating that lynx1, when expressed alone, does not bind to either protein G beads or to α_7-bound beads.

(B) Western blot probed with α_7 polyclonal antibody (upper panel) detects a specific band corresponding to α_7 at ~52 kDa in the I and IPα_7 fractions, indicating that α_7 mAb beads immunoprecipitate α_7 receptors. Incubation of the same blot with lynx1 antibody (lower panel) immunodetects lynx1 also in the I and IPα_7 fractions, demonstrating that lynx1 coimmunoprecipitates with α_7 receptors.

(C) Western blot probed with Flag-HRP antibody (upper panel) shows two specific bands corresponding to α_4 at ~69 kDa and β_2 at ~45 kDa subunits in I and IPα_4 fractions, indicating that α_4 mAb beads are able to immunoprecipitate both α_4 and β_2 molecules. The same blot incubated with lynx1 antibody (lower panel) immunodetects lynx1 in the precipitate fraction, demonstrating that lynx1 forms a stable complex with $\alpha_4\beta_2$ nicotinic receptors.

(D) Comparison of lanes I and IP$_{Flag}$ in the blot probed with anti-Flag antibody (upper panel) reveals an enrichment of both receptor types, $\alpha_4\beta_2$ nAChR and Grid2, in the precipitate fractions relative to the input fractions. Grid2 is indicated as δ_2 and migrates at ~114 kDa. The same blot incubated with lynx1 antibody (lower panel) shows that lynx1 is markedly enriched in the IP$_{Flag}$ fraction from cells coexpressing lynx1 with $\alpha_4\beta_2$ nicotinic receptors, but not from cells coexpressing lynx1 with the glutamate receptor Grid2, demonstrating the specificity of lynx1 coimmunoprecipitation with nicotinic receptors.

(E) Western blot probed with anti-Flag antibody (upper panel) reveals the two bands corresponding to α_4 and β_2 subunits in the I and IP$_{Flag}$ fractions. The same blot incubated with a PLAP antibody (lower panel) immunodetects PLAP in the input fraction, but not in the precipitate fraction, demonstrating that PLAP does not precipitate with $\alpha_4\beta_2$ nicotinic receptors.

greater extent in the presence of lynx1. Thus, rapid application of ACh was required to assess the consequences of lynx1 on single $\alpha_4\beta_2$ receptors. Using the outside-out patch mode of recording (Hamill et al., 1981), we locally perfused each patch with 100 μM ACh and observed single-channel currents due to $\alpha_4\beta_2$ receptors in both the presence and absence of lynx1 (Figure 4). In both the presence and absence of lynx1, ACh elicited an instantaneous flurry of channel activity that decayed in frequency over several seconds. However, in the presence of lynx1, the initial peak of channel activity decayed more rapidly and completely vanished within less than 10 s following the start of ACh application (Figure 4A). By contrast, without lynx1, channel events could be observed for tens of seconds following ACh application. These results suggest that lynx1 enhances the rate and extent of desensitization of $\alpha_4\beta_2$ nAChRs. Analysis of the current traces reveals that in the absence of lynx1, ACh elicits currents with three discrete amplitudes: large (A_{lg}), intermediate (A_{int}), and small (A_{sm}) (Figure 4A). Comparison of the current traces and quantitation using all-points histograms revealed a second effect of lynx1 on these receptors. In particular, lynx1 markedly increases the fraction of currents with large amplitude (Figure 4B). Computation of relative areas in the all-points histograms revealed an increase in the ratio of intermediate- to high-conductance channels from 1.0:0.22 in the absence of lynx1 (mean results from two patches) to 1.0:1.98 in the presence of lynx1 (mean results from four patches) or about a 10-fold increase. This shift toward larger current amplitude in the presence of lynx1 could reflect either an increase in the number of events with large amplitude or an increase in the mean duration of large amplitude events. No differences in the mean open duration could be detected for the large amplitude currents recorded in the absence or presence of lynx1 (Figure 4C). We conclude that lynx1 promotes large amplitude ACh-evoked currents through $\alpha_4\beta_2$ nAChRs. Thus, single-channel recordings reveal two novel neuromodulatory actions of lynx1 on $\alpha_4\beta_2$ nAChRs: enhancement of desensitization and promotion of large amplitude currents.

lynx1 Alters the Macroscopic Properties of nAChRs in *Xenopus* Oocytes

Single-channel recordings suggest that lynx1 enhances desensitization of $\alpha_4\beta_2$ nAChRs. However, due to slow rundown of nAChR channel events in isolated patches, quantitative effects of lynx1 on desensitization could not be determined. Thus, to quantify the effects of lynx1 on desensitization, we used the two-electrode voltage clamp to record macroscopic currents from *Xenopus* oocytes expressing $\alpha_4\beta_2$ nAChRs with or without lynx1. Following application of ACh, inward currents rapidly peaked and then decayed with a biphasic time course to a steady plateau current. This biphasic profile was observed regardless of whether lynx1 was coexpressed with $\alpha_4\beta_2$ receptors (Figure 5A) and is well-described by

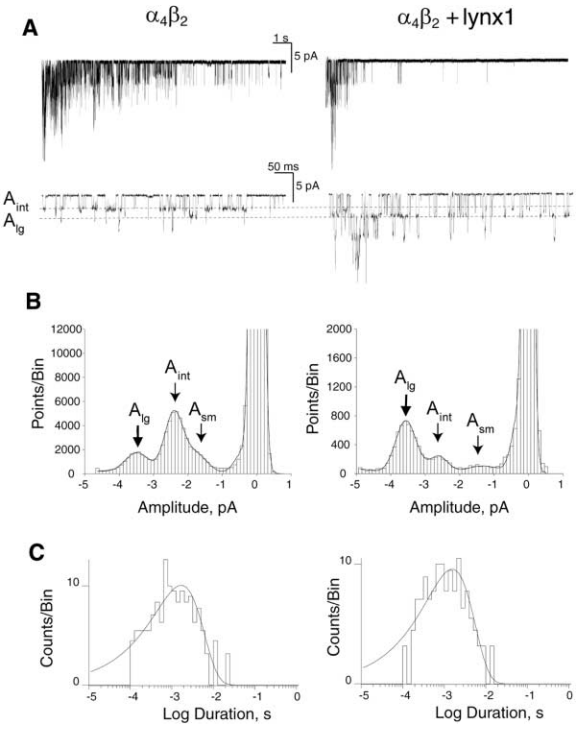

Figure 4. Single-Channel Currents through nAChRs Are Modulated by lynx1

Outside-out patches from BOSC cells were locally perfused with 100 μM ACh (see Experimental Procedures). Patches were formed from cells expressing either $\alpha_4\beta_2$ nAChRs (left column) or $\alpha_4\beta_2$ plus lynx1 (right column).

(A) Top traces show currents recorded immediately following ACh application and are displayed using a compressed time base. Lower traces show segments from the top traces on expanded time bases, with the largest (A_{lg}) and intermediate (A_{int}) current amplitudes indicated by the dotted lines.

(B) All-points histograms were obtained from the ACh-evoked currents from the entire trace for each recording; the truncated peaks at the far right correspond to baseline current, while the peaks to the left correspond to three amplitudes of unitary currents. Arrows indicate the largest (A_{lg}), intermediate (A_{int}), and smallest (A_{sm}) current amplitudes. For the data illustrated, normalized relative areas of large, intermediate, and small current amplitudes are as follows: $\alpha_4\beta_2$, 0.15/1.0/0.17; and $\alpha_4\beta_2$ plus lynx1, 1.0/0.3/0.21.

(C) Open-duration histograms for the large conductance currents, each fitted a single exponential (smooth curves); fitted time constants are: $\alpha_4\beta_2$, $\tau_0 = 1.8$ ms; and $\alpha_4\beta_2$ plus lynx1, $\tau_0 = 1.6$ ms. Qualitatively similar results were obtained for five patches from cells expressing $\alpha_4\beta_2$ and 19 patches from cells expressing $\alpha_4\beta_2$ plus lynx1.

the sum of two exponentials (corresponding to the fast and slow components) plus a constant. The rate of onset of desensitization was quantified by the value of the time constants, fast (τ_f) and slow (τ_s), obtained in the two-exponential fits (Figure 5B). The extent of desensitization was determined by the relative contribution of the fast component to the total decay (RC_f) (Figure 5C). Coexpression of lynx1 with $\alpha_4\beta_2$ significantly accelerated the τ_f ($\alpha_4\beta_2$: $\tau_f = 2.73 \pm 0.06$ s; $\alpha_4\beta_2$ plus lynx1: $\tau_f = 1.09 \pm 0.07$ s) with no alteration of τ_s (Figures 5A and 5B) and increased the RC_f (Figures 5A and 5C). Injection of lynx1 alone or coinjection of lynx1 with either α_4 or β_2 alone, yielded no detectable macroscopic currents in response to ACh (data not shown). These results indicate that lynx1 increases both the rate and extent of desensitization of $\alpha_4\beta_2$ receptors.

To ensure that the kinetic effects of lynx1 on $\alpha_4\beta_2$ receptors reflect a specific modulation of nAChRs by lynx1, three additional types of control experiments were conducted. First, the possibility that calcium-activated chloride currents contaminate the ACh-evoked currents under our recording conditions was tested. Oocytes were injected with the calcium chelator BAPTA (Figure 5D) or incubated with the membrane-permeant form BAPTA-AM (not shown) before recording. No differences were observed in either of these experiments when compared to untreated oocytes, either in the presence or absence of lynx1 (Figure 5A). Second, the specificity of lynx1 modulation of nAChRs was tested in coexpression studies of lynx1 and $GABA_A$ (γ-aminobutyric acid type A) receptors. GABA-evoked chloride currents were recorded from oocytes expressing $GABA_A$ receptors ($\alpha_1\beta_1\gamma_2$ combination) alone or together with lynx1 using voltage-clamp conditions. As shown in Figure 5E, no differences in the rate or extent of desensitization of $GABA_A$ receptors were observed. Further experiments at different GABA concentrations (1, 10, 100 μM and 1 mM GABA) revealed no differences in the fitted fast time constants (data not shown). Finally, the possibility that lynx1 might also change the capacitance of the oocyte membrane (Isom et al., 1995) was also examined. No change in membrane capacitance was observed between oocytes expressing $\alpha_4\beta_2$ receptors with or without lynx1 (217 ± 5 nF and 228 ± 3 nF, respectively, $n = 5$ oocytes) (data not shown). We conclude that the effect of lynx1 on the kinetics of desensitization of $\alpha_4\beta_2$ nAChRs reflects an important and novel modulatory role for lynx1 on these receptors. We previously reported that application of soluble lynx1 to $\alpha_4\beta_2$ receptors potentiated the ACh-evoked amplitude currents (Miwa et al., 1999). Since the efficiency of expression of the receptors from a given amount of injected cRNA varies between individual oocytes, we were not able to determine whether coinjected GPI-anchored lynx1 might also potentiate ACh-evoked currents. To determine whether soluble lynx1 might also have an effect on the rate of desensitization, we calculated the time constants of current decay in the original data set of experiments presented for soluble lynx1 application to $\alpha_4\beta_2$-expressing oocytes (Miwa et al., 1999). Two-exponential fit analysis of the ACh-evoked currents revealed that application of soluble lynx1 significantly accelerated the fast time constant (before lynx1 application, $\tau_f = 1.76 \pm 0.38$ s; during lynx1 application, $\tau_f = 0.93 \pm 0.2$ s, $n = 11$ oocytes). These data are consistent with an increase in nAChR desensitization in the presence of native GPI-anchored lynx1 reported here. However, since soluble lynx1 was applied as a pulse in these experiments and since the stability of its interaction with nAChRs is not known, the dissociation of soluble lynx1 from the receptors during the course of the experiments might also contribute to the kinetics of current decay.

To assess whether lynx1 affects ACh sensitivity of $\alpha_4\beta_2$ nAChRs, we applied different concentrations of ACh to oocytes expressing $\alpha_4\beta_2$ in the presence or absence of lynx1. In the presence of lynx1, $\alpha_4\beta_2$ receptors show reduced sensitivity to ACh, compared to $\alpha_4\beta_2$ alone (Figure 6A). Dose-response curves generated from the peak

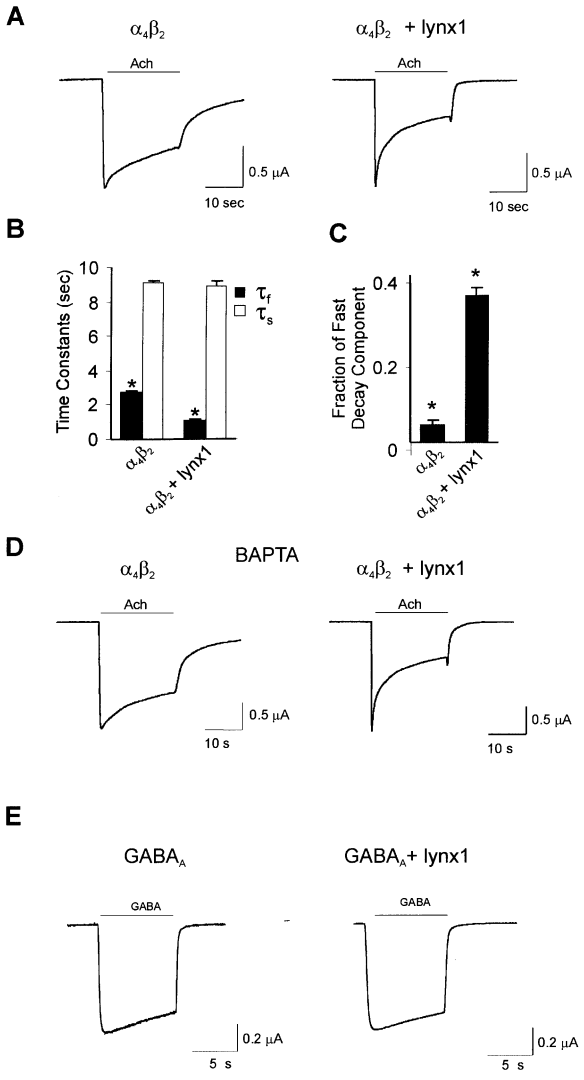

Figure 5. lynx1 Enhances Desensitization When Coexpressed with Nicotinic Receptors

(A) Enhanced onset and extent of desensitization during agonist application is observed when lynx1 is coexpressed with $\alpha_4\beta_2$ nicotinic receptors. Representative ACh-evoked currents in voltage-clamped *Xenopus* oocytes after coinjection of α_4 and β_2 cRNAs subunits with or without lynx1 cRNA. Inward currents were evoked by 20 s periods of superfusion (horizontal calibration bar), with external saline containing 1 mM ACh. The vertical calibration bars correspond to 0.5 μA.

(B and C) Bar graphs representing the values of the parameters obtained by fitting the two-exponential equation: $y(t) = [A_f \times \exp(-t/\tau_f)] + [A_s \times \exp(-t/\tau_s)] + C$ (τ_f and τ_s, fast and slow time constants; A_f and A_s, fraction of the fast and slow components; C, plateau current) to the inward current decay during agonist application. (B) Solid bars represent the values of τ_f and open bars correspond to τ_s. The values are: $\alpha_4\beta_2$, $\tau_f = 2.73 \pm 0.06$ s; $\alpha_4\beta_2$ plus lynx1, $\tau_f = 1.09 \pm 0.07$ s (Student's t test; $p = 1.4 \times 10^{-23}$) and $\alpha_4\beta_2$, $\tau_s = 9.14 \pm 0.05$ s; $\alpha_4\beta_2$ plus lynx1, $\tau_s = 8.96 \pm 0.24$ s. Values represent the mean ± SEM from 28 and 25 oocytes expressing $\alpha_4\beta_2$ and $\alpha_4\beta_2$ + lynx1, respectively. (C) Chart indicating the relative contribution of the fast decay component, RC_f, calculated as: $RC_f = A_f/(A_f + A_s + C)$. The values are: $\alpha_4\beta_2$, $RC_f = 0.06 \pm 0.01$; $\alpha_4\beta_2$ plus lynx1 $RC_f = 0.37 \pm 0.02$ (Student's t test; $p = 4.6 \times 10^{-15}$) and correspond to the mean ± SEM obtained from the same oocytes as above.

(D) No differences in the ACh-evoked responses were observed in control experiments to test for the activation of contaminating calcium-dependent currents. Representative ACh-evoked currents in oocytes expressing $\alpha_4\beta_2$ and $\alpha_4\beta_2$ plus lynx1 were injected with the calcium chelator BAPTA within 30 min before recording. Qualitatively similar results were obtained from 8 and 11 oocytes, respectively.

(E) Coexpression of lynx1 with $GABA_A$ receptors does not alter the desensitization kinetics of GABA-gated chloride currents. Representative GABA-evoked currents in voltage-clamped *Xenopus* oocytes after coinjection of α_1, β_1, and γ_2 $GABA_A$ receptor cRNAs subunits with or without lynx1 cRNA. Inward currents were evoked by 10 s periods of superfusion (horizontal calibration bar) with external saline containing 10 μM GABA. The vertical calibration bars correspond to 0.2 μA. Two-exponential fit analysis, as described in (B), indicated no significant change in the fitted time constants ($GABA_A$ receptor, $\tau_f = 5.02 \pm 0.04$ s and $\tau_s = 10.01 \pm 0.03$ s; $GABA_A$ receptor plus lynx1, $\tau_f = 5.13 \pm 0.15$ s and $\tau_s = 9.9 \pm 0.11$ s). Values represent the mean ± SEM from nine and seven oocytes expressing $GABA_A$ receptor or $GABA_A$ receptor plus lynx1, respectively.

currents reveal a shift of approximately 20-fold toward higher ACh concentrations in the presence of lynx1 (Figure 6B). From these results, we conclude that coexpression of lynx1 with $\alpha_4\beta_2$ nAChRs in oocytes increases the EC_{50} for ACh. To further investigate the effect of lynx1 on desensitization of $\alpha_4\beta_2$ receptors, we used a two-pulse protocol to examine the time course of recovery from desensitization induced by ACh. Figure 7A shows representative traces of the ACh-evoked currents elicited in oocytes expressing either $\alpha_4\beta_2$ (upper panel) or $\alpha_4\beta_2$ and lynx1 (lower panel) at increasing times following wash out of the initial desensitizing dose of ACh. At short time intervals following wash out of ACh (5–40 s), the peak amplitude of the second ACh-evoked current pulse is significantly reduced compared to the initial pulse in $\alpha_4\beta_2$ plus lynx1 coinjected oocytes, compared to $\alpha_4\beta_2$- expressing oocytes. The time course of recovery of the second pulse is described by a single exponential function in both cases. The corresponding time constant is significantly prolonged in oocytes expressing $\alpha_4\beta_2$ plus lynx1 (Figure 7B). These results indicate that lynx1 slows recovery from desensitization for $\alpha_4\beta_2$ receptors.

lynx1 shares the cysteine-rich consensus motif of the Ly6/neurotoxin superfamily. The disulfide bridges created by these conserved cysteines in α-neurotoxins create a rigid β sheet core from which three variable loops emerge (Tsetlin, 1999). To assess the structural specificity of lynx1 action on nAChRs we mutated several cysteines in lynx1 that might be critical for its overall topology. A schematic representation of lynx1, indicating its cysteine bridges, is shown in Figure 8A. We mutated single cysteines (lynx1 mutants C4, C5, C7, and C9) or two cysteines (lynx1 mutants C2C3 and C6C7) to alanine to test the importance of each disulfide bond. We coexpressed each lynx1 mutant with $\alpha_4\beta_2$ nAChRs and examined the desensitization during application of ACh, as described in Figure 4C. No enhancement in the extent of desensitization was observed with lynx1 mutants C2C3, C4, and C6C7 (Figure 8B). In contrast, coexpression of lynx1 mutants C5, C7, and C9 with $\alpha_4\beta_2$ receptors caused a similar enhancement of the rapidly decaying component to that observed with wild-type lynx1 (Figure 8B). To rule out the possibility that functional differences between lynx1 and lynx1 mutants were due to differential expression of the lynx1 molecules, extracts from

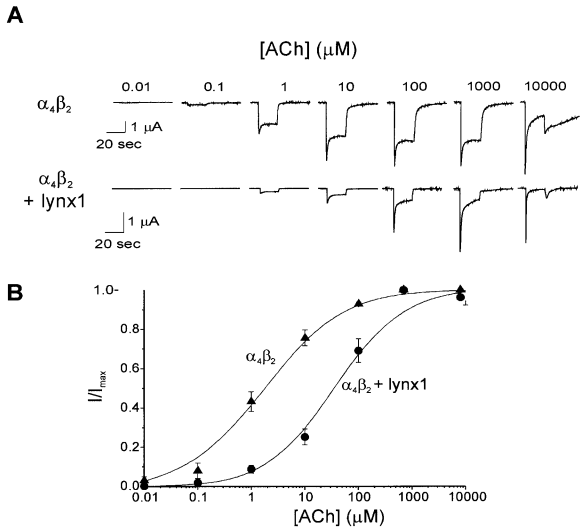

Figure 6. nAChRs Show Altered Sensitivity to ACh When Coexpressed with lynx1

(A) Representative currents induced in *Xenopus* oocytes after coinjection of α_4 and β_2 cRNAs nAChR subunits with or without lynx1 cRNA. Responses to consecutive applications of increasing concentrations of ACh are displayed for both $\alpha_4\beta_2$ (upper panel) and $\alpha_4\beta_2$ with lynx1 (lower panel). Inward currents were evoked by 20 s periods of superfusion (horizontal calibration bar) with external saline-containing ACh at the concentrations indicated above each trace. The vertical calibration bars correspond to 1 μA.

(B) Concentration-response curves for ACh on oocytes expressing $\alpha_4\beta_2$ (closed triangle) and $\alpha_4\beta_2$ nAChRs with lynx1 (closed circle). The dependence of the peak inward amplitude response on the concentration of ACh was normalized to the peak amplitude of control responses induced by 1 mM ACh. Each plotted value is the mean ± SEM obtained from seven oocytes. Each ACh concentration point was tested by three consecutive pulses. The data obtained were fitted to the following form of the Hill equation: $I/I_{max} = [ACh]^{nH}/([ACh]^{nH} + (EC_{50})^{nH})$ (drawn lines). The fitted parameters are: $\alpha_4\beta_2$, $EC_{50} = 1.8 \pm 0.3$ μM and $nH = 0.71 \pm 0.04$; $\alpha_4\beta_2$ plus lynx1, $EC_{50} = 35 \pm 3.9$ μM and $nH = 0.82 \pm 0.03$.

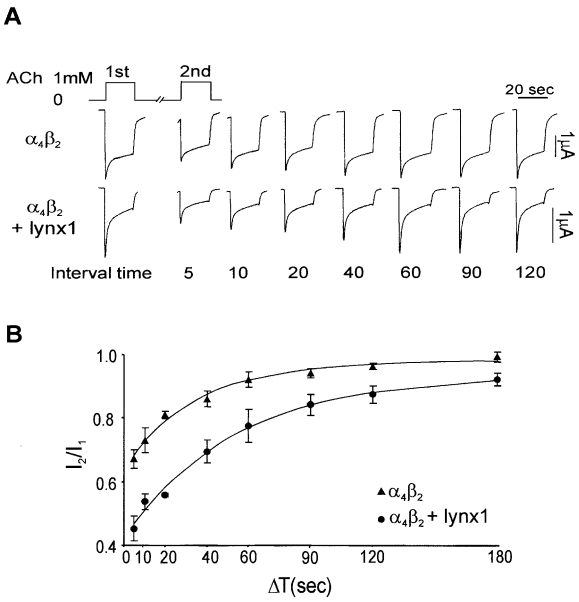

Figure 7. nAChRs Show Slower Recovery Rate When Coexpressed with lynx1

(A) Representative traces obtained in a two-pulse experiment measuring the time course of recovery of ACh-evoked currents in oocytes injected with $\alpha_4\beta_2$ (upper panel) or with $\alpha_4\beta_2$ plus lynx1 (lower panel). Two consecutive pulses of ACh (1 mM) were given at the intervals indicated below each trace. Horizontal and vertical calibration bars indicate the duration of the agonist application and the magnitude of the currents, respectively.

(B) The relative peak amplitudes (I_2/I_1) measuring the recovery time course of ACh-evoked currents in oocytes expressing $\alpha_4\beta_2$ nAChRs (closed triangle) and $\alpha_4\beta_2$ nAChRs with lynx1 (open circle). Each value is the mean ± SEM of four oocytes in each case. The continuous curves are fits of a single exponential of the form: $I_2/I_1 = [C_1 \times \exp(-t_{int}/\tau_{rec})] + C_2$, where I_1 and I_2 are the peak amplitude responses of the first and second ACh pulses, C_1 and C_2 are constants, t_{int} is the length of the interval time, and τ_{rec} is the recovery time rate. The relative peaks (I_2/I_1) recover with the fitted time constants: $\alpha_4\beta_2$, $\tau_{rec} = 32 \pm 2$ s; $\alpha_4\beta_2$ plus lynx1, $\tau_{rec} = 53 \pm 5$ s (Student's t test; $p = 1.8 \times 10^{-3}$).

injected oocytes were examined by immunoblotting with a lynx1 antibody. No significant differences in expression of lynx1 mutants were observed (Figure 8C). These results demonstrate that the disulfide bridges C2-C3 and C4-C6 are required for lynx1 to promote desensitization of ACh-evoked currents through $\alpha_4\beta_2$ nAChRs.

Discussion

The present results establish that lynx1 functions as a novel modulator of neuronal nAChRs. lynx1 colocalizes with both $\alpha_4\beta_2$ and α_7 nAChRs on a variety of neuronal subtypes in mouse brain, and it stably associates with these receptors in cultured mammalian cells. We find that coexpression of lynx1 with $\alpha_4\beta_2$ nAChRs shifts the distribution of current amplitudes to a more uniform and larger amplitude, increases the EC_{50} for ACh-evoked currents, and alters the kinetics and extent of desensitization. Because mutations in neuronal nAChRs that affect their kinetics severely impair CNS function, our results strongly suggest that lynx1 may play an important role in modulating central cholinergic function.

Previous studies of $\alpha_4\beta_2$ nAChRs demonstrated high and low EC_{50}s for ACh and that the low concentration EC_{50} was associated with receptors with slow desensitization onset (Buisson et al., 2000; Buisson and Bertrand, 2001); fast and slow rates of desensitization onset have also been observed (Buisson et al., 1996). Furthermore, two predominant current amplitudes were observed (Kuryatov et al., 1997; Buisson and Bertrand, 2001). Our results show a similar association between the low ACh concentration EC_{50} and slow desensitization, and our two predominant current amplitudes coincide with those previously observed.

Coexpression of lynx1 with $\alpha_4\beta_2$ nAChRs leads to a more homogeneous distribution of current amplitudes, with the large amplitude currents predominating, but lynx1 does not affect the kinetics of channel closing. Coincident with the shift in current amplitude is a shift to a high ACh concentration EC_{50} and enhancement of desensitization. Thus, the modulatory effect of lynx1 maintains the $\alpha_4\beta_2$ nAChR in the high-conductance, high-EC_{50}, and strongly desensitizing conformation. Because no single underlying mechanism relates current amplitude, EC_{50} and desensitization, we conclude that

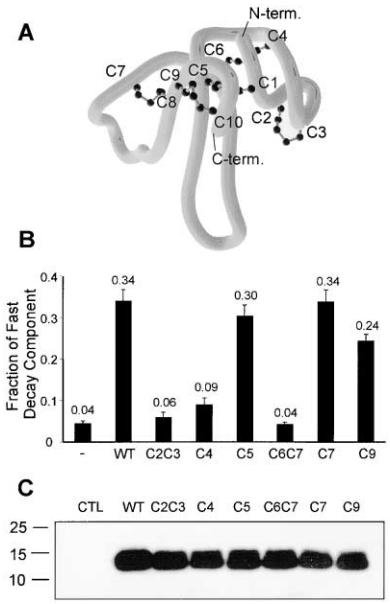

Figure 8. Mutation of Individual Cysteines Indicate that Two of the Five Cysteine Bridges in lynx1 Are Critical for Its Activity

(A) Three-dimensional model of lynx1 showing the five disulfide bridges and the C and N termini of the molecule. The cysteine bonds are between cysteines 1 and 5, cysteines 2 and 3, cysteines 4 and 6, cysteines 7 and 8, and cysteines 9 and 10.

(B) Single cysteines (lynx1 mutants C4, C5, C7, and C9) or two cysteines (lynx1 mutants C2C3 and C6C7) were mutated to alanines in lynx1 to test the importance of each disulfide bond. The ACh-gated currents obtained from oocytes coinjected with only $\alpha_4\beta_2$ nAChRs (−) with $\alpha_4\beta_2$ and wild-type lynx1 (wt) or with $\alpha_4\beta_2$ and lynx1 mutants (C2C3, C4, C5, C6C7, C7, and C9) were analyzed for differences in the relative contribution of the fast decay component (RC_f), as described in Figure 5C. The values obtained are plotted in the bar graph. Each value is the mean ± SEM of seven to 12 oocytes.

(C) Western blot analysis of lynx1 immunodetected protein on oocytes injected with lynx1 or lynx1 mutants. Extracts from uninjected control oocytes (CTL) were loaded in lane 1. Extracts from oocytes injected with wild-type lynx1 (wt) or with the different lynx1 cysteine mutants (C2C3 to C9) are loaded in the following lanes.

the action of lynx1 arises through a profound global change in receptor conformation.

Whereas lynx1 appears to function by maintaining low ACh sensitivity, a high signal to noise ratio, and a good safety margin to ACh exposure, chronic exposure to nicotine opposes maintenance of this multifaceted functional state. Nicotine exposure shifts the EC_{50} to low ACh concentrations, slows the onset of desensitization, and increases the number of high-affinity epibatidine binding sites (Buisson and Bertrand, 2001). These effects are not due to changes in receptor mRNA expression (Marks et al., 1992) or to changes in the concentration of receptors in the membrane (Whiteaker et al., 1998). Rather, it has been proposed that long-term exposure to nicotine induces an isomerization of nAChRs from a low- to a high-affinity state (Buisson and Bertrand, 2001). The effect of chronic nicotine exposure on single-channel conductance remains to be fully examined, but the two predominant current amplitudes characteristic of $\alpha_4\beta_2$ nAChRs were observed without nicotine exposure, as well as following upregulation with the competitive antagonist dihydro-β-erythroidine (Buisson and Bertrand, 2001). Our overall results suggest that lynx1 opposes the changes in functional properties induced by chronic exposure to nicotine. Thus, lynx1 might be important in the response to chronic nicotine exposure in vivo.

The major effects of lynx1 modulation of nicotinic receptors are to change a wide spectrum of functional properties of $\alpha_4\beta_2$ receptors. Mutations in human α_4 and β_2 subunits have been genetically linked to autosomal dominant nocturnal frontal lobe epilepsy (ADNFLE) (Steinlein et al., 1995; Phillips et at., 2001). Effects of these mutations on $\alpha_4\beta_2$ receptors show that they also strongly affect the kinetic properties of the receptors in vitro, leading to increased desensitization, slowed recovery, impaired calcium permeability, and changes in the single-channel conductance (Weiland et al., 1996; Kuryatov et al., 1997; Figl et al., 1998). Since alterations of this nature have important neurological effects, the actions of lynx1 on some of these aspects of nicotinic receptor activity point to an important role for lynx1 in nervous system function.

Our data demonstrate that lynx1 can form a stable complex with nicotinic receptors and that it colocalizes with these receptors in neurons. Although we do not yet know all the receptors lynx1 can modulate, our results establish preferential binding to α_7 and $\alpha_4\beta_2$ nAChRs. This physical association indicates that lynx1 could potentially alter the function of these receptors in vivo. The attachment of lynx1 to the cell surface by a GPI-anchor and its somatodendritic localization have important implications regarding the mechanism of lynx1 action. Unlike conventional secreted neurotoxins and neuromodulatory proteins, lynx1 action may operate on receptors present in the same subcellular domains. Localization of lynx1 to the cell membrane can allow it to be presented at a high local concentration to its target receptors to facilitate biologically robust effects. It also presents opportunities for dynamic modulation of receptors at the cell surface that would not be available to secreted modulatory proteins. Furthermore, since GPI-anchors are covalently attached in the endoplasmic reticulum and the modified proteins are transported through the secretory pathway to the cell surface, lynx1 also has the opportunity to associate with receptors during assembly and transport. Previous studies on the functional characterization of nAChRs have shown that variations in subunit type and α:β stoichiometry can affect the rate of decay and EC_{50} of ACh-evoked currents (Ramirez-LaTorre et al., 1996; Gerzanich et al., 1998; Zwart and Vijverberg, 1998). It has been proposed that some of these structural changes can influence the ability of the receptor to make concerted changes in conformation that are required for channel opening or desensitization. If lynx1 can act during processing and transport of receptors to the cell surface, one might expect that those receptors reaching the cell surface represent a limited subset of all possible combinations available, based on subunit expression profiles. In this case, the role of lynx1 could be to enhance the uniformity of the cellular response to ACh by selecting specific forms of the receptor to be presented at the cell surface, thereby modulating the functional response of these receptors. Alternatively, lynx1 could enhance the rate of assembly

of nAChR subunits and/or increase the probability of insertion into the membrane. Although these mechanisms could account for some of the effects of lynx1, it is evident that the role of lynx1 is not to act solely as a chaperone, as lynx1 can be found in high quantities at the cellular periphery. Indeed, we have previously reported that lynx1 can increase macroscopic currents when applied in soluble form, demonstrating its ability to act on preformed α_7 and $\alpha_4\beta_2$ receptors.

In conclusion, we present strong evidence demonstrating that lynx1 can modulate important properties of nAChRs. lynx1 is present in the same cellular locations as neuronal nicotinic receptors, it can directly associate with these receptors, and alter their responses to ACh. Studies of mice carrying *lynx1* null mutations will allow us to further establish a role for this modulator in CNS function in mammals. The existence of many *lynx1*-like CNS expressed genes in the mammalian and invertebrate genomes (our unpublished data), the novel mechanistic properties of lynx1 that we have reported here, and the demonstration that a *lynx1*-like gene (*odr-2*) is expressed at high levels in sensory and motor neurons in *C. elegans* and is required for chemotaxis in response to olfactory cues (Chou et al., 2001) support the idea that this class of neuromodulatory proteins may have diverse roles in the CNS.

Experimental Procedures

Constructs

The cDNA sequence encoding mouse lynx1 flanked by its 3′ and part of its 5′ untranslated sequences was subcloned into the oocyte expression vector pCS2+ and used for in vitro transcription and transfection experiments. lynx1 cysteine mutants were prepared using the Quick-Change Site-Directed Mutagenesis kit (Stratagene, La Jolla, CA). All mutations were verified by sequencing. cDNAs encoding nAChR α_4, β_2, and α_7 subunits were a gift from Dr. Marc Ballivet. The cDNAs of the $GABA_A$ receptor subunits α_1, β_1, and γ_2 were a gift from Dr. Myles Akabas. The constructs containing α_7 and Flag-tagged α_4 and β_2 nAChR cDNAs were a gift from Dr. José Ramirez-LaTorre. The expression plasmid containing the cDNA of the delta 2 glutamate receptor (Grid2) (Zuo et al., 1997) was Flag-tagged at the N terminus by Dr. Zhenyu Yue. The GPI-anchored PLAP expression plasmid was constructed by Dr. Toshifumi Tomoda.

Antibodies

The rabbit polyclonal antibody against the nAChR α_4 subunit was a kind gift from Dr. Scott Rogers. The monoclonal antibodies FlagM2, mAb 306 anti-α_7, mAb 299 anti-α_4, and HRP-coupled anti-Flag antibodies were purchased from SIGMA. The polyclonal antibody anti-α_7 was purchased from Santa Cruz Antibodies. Fluorescent-conjugated and HRP-conjugated secondary antibodies were purchased from Jackson Immunochemicals. The rabbit polyclonal antibody against human PLAP was purchased from ZYMED. The rabbit polyclonal antibody against lynx1 was obtained as described in Miwa et al. (1999) and was affinity purified on a cyanogen bromide activated Sepharose 4B column (Sigma-Aldrich) coupled to the lynx1 peptide TTRTYFTPYRMKVRKS according to the manufacturer instructions.

Monoclonal Antibody Production

A lynx1-his epitope fusion protein was prepared from BL21(DE3)-pLys cells transformed with pET264 plasmid constructed by subcloning mature, secreted lynx1 (without the signal sequence or GPI-anchor sequence) into the XhoI site of the pET14b bacterial expression vector (Novagen). IPTG-induced cell lysates were denatured in 8 M Urea, purified on nickel beads (Qiagen), and renatured by sequential 2-fold dilutions in PBS. This lynx1-his fusion protein was injected into mice (Green Mountain Antibodies, Burlingtion, VT), and monoclonal cell lines were screened by Western blot analysis, immunofluorescence analysis on cells transfected with a CMV-lynx1 plasmid, and immunocytochemical analysis on mouse brain sections. Ascites fluid against this cell line (lynx1-1) was purified on a ProA column to a final concentration of 17 mg/ml.

Immunohistochemistry

Experiments were done using a monoclonal antibody (mAb 8589) and an affinity-purified polyclonal antibody against lynx1, an anti-α_4 nAChR polyclonal serum (Flores et al., 1992), and a monoclonal against α_7 nAChR (mAb 306, SIGMA). 1-month-old mice (Inbred F1 hybrid CBA/J $\times$ C57Bl/6) were perfused with saline, 0.2% paraformaldehyde/PBS, and 2% paraformaldehyde/5% sucrose/PBS. Dissected brains were sectioned at 50 μm on a freezing microtome. Double-immunofluorescence experiments with lynx1 and α_4 nAChR were done by incubating free-floating sections with α_4 antiserum at a 1:1600 dilution overnight at 4°C, washing and subsequent incubation with anti-rabbit Cy3-conjugated antibody for 1 hr at RT. Next, sections were extensively washed, processed following the M.O.M. kit (Vector Lab) instructions, and incubated with lynx1 mAb 8589 at a 1:30,000 dilution for 1 hr at 4°C, washed, and incubated with Cy5-conjugated anti-mouse antibody for 1hr at RT. Double-immunofluorescence experiments with lynx1 and α_7 nAChR were done using the affinity-purified polyclonal antibody against lynx1 diluted 1:10 and Cy3-conjugated goat anti-rabbit antibody, followed by incubation with α_7 mAb 306 according to M.O.M. (Vector Lab) manufacturer instructions at a 1:100 dilution and Cy5-conjugated anti-mouse antibody. Sections were mounted on microscope slides and imaged on a BioRad Radiance 2000 confocal microscope.

Expression and Immunoprecipitation from HEK 293T Cells

HEK 293T cells were transfected by calcium phosphate precipitation with the expression vectors containing the cDNAs of lynx1, α_7 nAChR, Flag-tagged α_4 and β_2 nAChR subunits, Flag-tagged Grid2, and GPI-linked PLAP . Two days after transfection, cells were washed with PBS, harvested in lysis buffer (150 mM NaCl, 50 mM HEPES, 100 mM PMSF, 1.5 μg/ml aprotinin, 10 μg/ml leupeptin, and protease inhibitor cocktail) containing 1% Triton X-100 and centrifuged at 14,000 rpm for 5 min. Insoluble cell pellets were resuspended in lysis buffer containing 1% NP40 and 0.05% deoxycholate for 3 hr at 4°C and precleared by centrifugation at 14,000 rpm for 5 min. Protein G agarose beads (Roche) were used as described by the manufacturer. Essentially, G beads were incubated with either no antibody or monoclonal antibodies mAb 306, mAb 299, or Flag M2 in NP40/deoxycholate lysis buffer for 3 hr at 4°C with gentle rocking. Antibody-bound protein G beads were centrifugated at 5000 rpm for 1 min, supernatants were removed, and the precleared transfected cell extracts were incubated with the antibody-bound G beads overnight at 4°C with gentle rocking. Agarose beads were extensively washed with NP40/deoxycholate lysis buffer and resuspended in 4$\times$ reducing sample buffer (Invitrogen). Cell extracts and protein G fractions were loaded on SDS-PAGE gels (Invitrogen) and transferred to PVDF membranes (Immobilon P, Millipore). Blots were blocked with 5% nonfat milk in PBS with 0.1% Tween-20 for 30 min and incubated with either polyclonal α_7 antibody (Santa Cruz), HRP-coupled anti-Flag antibody (SIGMA), or affinity-purified anti-lynx1 polyclonal antibody overnight at 4°C. Westerns incubated with α_7 and lynx1 antibodies were washed in blocking solution and incubated with the corresponding HRP-conjugated secondary antibodies in blocking solution. Blots were extensively washed and developed by cheminoluminiscence using ECL (NEN Biolabs).

Receptor Expression in BOSC Cells and Recordings of ACh-Evoked Single-Channel Currents

BOSC cells were transfected by calcium phosphate precipitation as described above (Wang et al., 2000). BOSC cells are a cell line variant of the HEK 293T cell line (Pear et al., 1993). nAChR cDNAs were cotransfected with the cDNA encoding Green Fluorescent protein to facilitate identification of transfected cells. Transfected cells were bathed in depolarizing buffer containing 142 mM KCl, 5.4 mM NaCl, 1.8 mM $CaCl_2$, 1.7 mM $MgCl_2$, 10 mM HEPES (pH 7.4) and cell-free outside-out patches were formed as described (Hamill et

al., 1981) using the patch pipette buffer 80 mM KF, 20 mM KCl, 40 mM K aspartate, 2 mM $MgCl_2$, 1 mM EGTA, 10 mM HEPES (pH 7.4). To avoid desensitization, a second pipette containing 100 μM ACh in depolarizing buffer was positioned near the isolated patch immediately before recording, and ACh was applied by pressure injection. ACh-evoked currents were recorded with an Axoclamp 200B, digitized at 100 kHz using the program Acquire, and filtered at 2 kHz for analysis of all-points and open-time histograms using the program TAC (Bruxton Corp.)

Expression of nAChRs and lynx1 in *Xenopus* Oocytes

The cRNAs for lynx1, lynx1 cysteine mutants, nAChR subunits (α_4 and β_2), and $GABA_A$ receptor subunits (α_1, β_1, and γ_2) were synthesized in vitro using T7 or SP6 RNA polymerases (mMESSAGE mMACHINE, Ambion, Austin, TX) after linearization. To quantify the yield of the synthesized transcripts, a radiolabeled nucleotide tracer was included in the reaction, and the rate of incorporation was determined with a scintillation counter. The synthesized cRNAs were also measured by spectophotometer and checked by formaldehyde agarose gel. *Xenopus* oocytes were surgically removed from adult *X. laevis* and incubated in 2 mg/ml collagenase (Type I, Sigma-Aldrich) in ND-96 (Specialty Media) for 3 hr at RT. Oocytes were then washed four times with Barth's medium (Specialty Media), transferred to L-15 medium (Specialty Media), and allowed to recover at 18°C overnight before cRNA injection. Oocytes were injected with 0.5 ng of the cRNA encoding each nAChR subunit or $GABA_A$ subunit and 3 ng of lynx1. The volume injected was 20 nl per oocyte. α, β, and γ subunits were injected in 1:1 ratios. Oocytes were maintained semisterile in L-15 medium at 18°C after cRNA injection, and recordings were performed between 1 and 2 days after injection.

Electrophysiological Recordings from Oocytes, Data Acquisition, and Analysis

Macroscopic currents were recorded with a GeneClamp 500B amplifier (Axon Instruments) using a two-electrode voltage clamp with active ground configuration. Electrodes were filled with 3 M KCl and had resistances of 0.5 to 2 MΩ. All recordings were digitized (DigiData 1200 Series Interface, Axon Instruments) at a sampling rate of 11.7 ms per point and data were acquired using pCLAMP6 software (Axon Instruments) and filtered at 10 Hz. Membrane potential was clamped to −70 mV; only oocytes with leak currents <100 nA were used. The extracellular recording solution contained: 82.5 mM NaCl, 2 mM KCl, 1 mM $CaCl_2$, 1 mM $MgCl_2$, 10 mM HEPES, and 1 μM atropine (pH 7.5) (all reagents from Sigma-Aldrich). BAPTA control experiments were performed either (1) by injection of oocytes with 40 nl of 100 mM BAPTA salt (Sigma), resuspended in 85 mM Na^+, 2.5 mM K^+, and 10 mM HEPES adjusted to pH 7.4 within 30 min before recording or (2) by incubation in L-15 medium (Specialty Media) containing 100 μM BAPTA-AM (Sigma) resuspended in DMSO for 3–4 hr before recording. ACh and GABA (RBI) were prepared in extracellular solution at concentrations of 10 nM to 10 mM. Control perfusion solution or agonist-containing solutions were gravity fed using a Bath Perfusion System valve controller (BPS-8, Ala Scientific Instruments), activated by TTL input, and modified such that no mixing between solutions occurred (the two manifolds were removed and the tubing from each reservoir was directly plugged in the recording chamber). Oocytes were perfused at ~5 ml/min and the time delay between beginning of the application and first deflection of the induced current was typically 0.5 s. Oocytes were exposed to applications of ACh or GABA separated by at least 5 min interval. Capacitance measurements were recorded at a sampling rate of 200 μs per point (5 Hz). Capacity transients resulting from a 20 mV voltage jump (from −70 mV to −50mV and back) were integrated to obtain the total charge accumulated across the membrane. The total oocyte capacitance was estimated using the equation $C = Q/\Delta V$. Graphical and statistical analyses were done using Microsoft Excel and Origin 5.0.

Western Analysis of lynx1 Mutants in *Xenopus* Oocytes

Oocytes were injected with 15–18 ng of cRNA synthesized from lynx1 or lynx1 cysteine mutants constructs and maintained in L-15 medium for 2 days. The amount of lynx1 or lynx1 cysteine mutants cRNA injected for these expression control experiments was 5–6 times greater than that used in two-electrode voltage clamp experiments. Injected oocytes were homogeneized in oocyte lysis buffer (10% glycerol, 1% Triton X-100, 100 mM PMSF, 1.5 μg/ml aprotinin, and 10 μg/ml leupeptin in extracellular recording solution). Typically, 20 oocytes were homogeneized in 100 μl lysis buffer. Homogenates were centrifuged for 20 min at 14,000 rpm and the intermediate phase was collected. Oocyte extracts (15 μl) were run in a PAGE gel (Novex) and Western blotting was performed as indicated before.

Acknowledgments

We thank Scott Rogers for the rabbit polyclonal antibody against mouse α_4 nAChRs; Marc Ballivet, José Ramirez-LaTorre, and Myles Akabas for the expression plasmids encoding nAChR and GABA receptor subunit cDNAs; and Zhenyu Yue and Toshifumi Tomoda for the Grid and PLAP expression plasmids, respectively. We are grateful to Lorna W. Role for her scientific expertise and advice during the course of this study and her thoughtful comments on the manuscript. We would like to thank Paola Vergani for her help with the capacitance measurements, and together with Pablo Artigas, Lain F. Diaz, and David C. Gadsby for their expert advice and valuable discussions. We would like to acknowledge Daniel Besser for critical reading of the manuscript and helpful discussions and Ali Hemmati-Brivanlou, Chenbei B. Chang, and Kathy Zimmerman for help with the injection of *Xenopus* oocytes. This research was supported by the Howard Hughes Medical Institute, NIH NINDS P01 NS30532; AT Children's Project and HHMI (I.I.-T.); The Rockefeller University and NIH CA 09673 (J.M.M.); NS-22061 (to L.W. Role for support of G.W.C.) and NS-31744 (S.M.S.).

Received: December 1, 2000
Revised: December 18, 2001

References

Buisson, B., and Bertrand, D. (2001). Chronic exposure to nicotine upregulates the human $\alpha_4\beta_2$ nicotinic acetylcholine receptor function. J. Neurosci. *21*, 1819–1829.

Buisson, B., Gopalakrishnan, M., Arneric, S., Sullivan, J., and Bertrand, D. (1996). Human $\alpha4\beta2$ neuronal nicotinic acetylcholine receptor in HEK293 cells: a patch clamp study. J. Neurosci. *16*, 7880–7891.

Buisson, B., Vallejo, Y., Green, W., and Bertrand, D. (2000). The unusual nature of epibatidine responses at the $\alpha4\beta2$ nicotinic acetylcholine receptor. Neuropharmacology *39*, 2561–2569.

Changeux, J.P., Bertrand, D., Corringer, P.J., Dehaene, S., Edelstein, S., Lena, C., Le Novere, N., Marubio, L., Picciotto, M., and Zoli, M. (1998). Brain nicotinic receptors: structure and regulation, role in learning and reinforcement. Brain Res. Brain Res. Rev. *26*, 198–216.

Chou, J.H., Bargmann, C.I., and Sengupta, P. (2001). The *Caenorhabditis elegans* odr-2 gene encodes a novel Ly-6-related protein required for olfaction. Genetics *157*, 211–224.

Dominguez del Toro, E., Juiz, J.M., Peng, X., Lindstrom, J., and Criado, M. (1994). Immunocytochemical localization of the alpha 7 subunit of the nicotinic acetylcholine receptor in the rat central nervous system. J. Comp. Neurol. *349*, 325–342.

Everitt, B.J., and Robbins, T.W. (1997). Central cholinergic systems and cognition. Annu. Rev. Psychol. *48*, 649–684.

Elgoyhen, A.B., Vetter, D.E., Katz, E., Rothlin, C.V., Heinemann, S.F., and Boulter, J. (2001). Alpha 10: a determinant of nicotinic cholinergic receptor function in mammalian vestibular and cochlear mechanosensory hair cells. Proc. Natl. Acad. Sci. USA *98*, 3501–3506.

Figl, A., Viseshakul, N., Shafaee, N., Forsayeth, J., and Cohen, B.N. (1998). Two mutations linked to nocturnal frontal lobe epilepsy cause use-dependent potentiation of the nicotinic ACh response. J. Physiol. *513*, 655–670.

Flores, C.M., Rogers, S.W., Pabreza, L.A., Wolfe, B.B., and Kellar, K.J. (1992). A subtype of nicotinic cholinergic receptor in rat brain is composed of alpha 4 and beta 2 subunits and is up-regulated by chronic nicotine treatment. Mol. Pharmacol. *41*, 31–37.

Gerzanich, V., Wang, F., Kuryatov, A., and Lindstrom, J. (1998). Alpha

5 subunit alters desensitization, pharmacology, Ca^{2+} permeability and Ca^{2+} modulation of human neuronal alpha 3 nicotinic receptors. J. Pharmacol. Exp. Ther. *286*, 311–320.

Grant, G.A., Luetje, C.W., Summers, R., and Xu, X.L. (1998). Differential roles for disulfide bonds in the structural integrity and biological activity of kappa-Bungarotoxin, a neuronal nicotinic ACh receptor antagonist. Biochemistry *35*, 12166–12171.

Hall, Z.W. (1999). Alpha neurotoxins and their relatives: foes and friends? Neuron *23*, 4–5.

Hamill, O.P., Marty, A., Neher, E., Sakmann, B., and Sigworth, F.J. (1981). Improved patch-clamp techniques for high-resolution current recording from cells and cell-free membrane patches. Pflugers Arch. *391*, 85–100.

Hill, J.A., Zoli, M., Bourgeois, J.P., and Changeux, J.P. (1993). Immunocytochemical localization of a neuronal nicotinic receptor: the beta 2-subunit. J. Neurosci. *13*, 1551–1568.

Horie, M., Okutomi, K., Taniguchi, Y., Ohbuchi, Y., Suzuki, M., and Takahashi, E. (1998). Isolation and characterization of a new member of the human Ly6 gene family (LY6H). Genomics *53*, 365–368.

Kuryatov, A., Gerzanich, V., Nelson, M., Olale, F., and Lindstrom, J. (1997). Mutation causing autosomal dominant nocturnal frontal lobe epilepsy alters Ca^{2+} permeability, conductance, and gating of human alpha4beta2 nicotinic ACh receptors. J. Neurosci. *17*, 9035–9047.

Isom, L.L., Ragsdale, D.S., De Jongh, K.S., Westenbroek, R.E., Reber, B.F., Scheuer, T., and Catterall, W.A. (1995). Structure and function of the beta 2 subunit of brain sodium channels, a transmembrane glycoprotein with a CAM motif. Cell *83*, 433–442.

Lindstrom, J. (1997). Nicotinic ACh receptors in health and disease. Mol. Neurobiol. *15*, 193–222.

Lukas, R.J., Changeux, J.P., Le Novere, N., Albuquerque, E.X., Balfour, D.J., Berg, D.K., Bertrand, D., Chiappinelli, V.A., Clarke, P.B., Collins, A.C., et al. (1999). International Union of Pharmacology. XX. Current status of the nomenclature for nicotinic ACh receptors and their subunits. Pharmacol. Rev. *51*, 397–401.

Marks, M.J., Pauly, J.R., Gross, S.D., Deneris, E.S., Hermans-Borgmeyer, I., Heinemann, S.F., and Collins, A.C. (1992). Nicotine binding and nicotinic receptor subunit RNA after chronic nicotine treatment. J. Neurosci. *12*, 2765–2784.

Miwa, J.M., Ibañez-Tallon, I., Crabtree, G.W., Sánchez, R., Šali, A., Role, L.W., and Heintz, N. (1999). lynx1, an endogenous toxin-like modulator of nicotinic ACh receptors in the mammalian CNS. Neuron *23*, 105–114.

Nakayama, H., Shioda, S., Okuda, H., Nakashima, T., and Nakai, Y. (1995). Immunocytochemical localization of nicotinic ACh receptor in rat cerebral cortex. Brain Res. Mol. Brain Res. *32*, 321–328.

Pear, W.S., Nolan, G.P., Scott, M.L., and Baltimore, D. (1993). Production of high-titer helper-free retroviruses by transient transfection. Proc. Natl. Acad. Sci. USA *90*, 8392–8396.

Phillips, H.A., Favre, I., Kirkpatrick, M., Zuberi, S.M., Goudie, D., Heron, S.E., Scheffer, I.E., Sutherland, G.R., Berkovic, S.F., Bertrand, D., and Mulley, J.C. (2001). CHRNB2 is the second acetylcholine receptor subunit associated with autosomal dominant nocturnal frontal lobe epilepsy. Am. J. Hum. Genet. *68*, 225–231.

Ramirez-Latorre, J., Yu, C.R., Qu, X., Perin, F., Karlin, A., and Role, L. (1996). Functional contributions of alpha5 subunit to neuronal ACh receptor channels. Nature *380*, 347–351.

Rogers, S.W., Gahring, L.C., Collins, A.C., and Marks, M. (1998). Age-related changes in neuronal nicotinic ACh receptor subunit alpha4 expression are modified by long-term nicotine administration. J. Neurosci. *18*, 4825–4832.

Role, L.W., and Berg, D.K. (1996). Nicotinic receptors in the development and modulation of CNS synapses. Neuron *16*, 1077–1085.

Schoepfer, R., Conroy, W.G., Whiting, P., Gore, M., and Lindstrom, J. (1990). Brain alpha-bungarotoxin binding protein cDNAs and mAbs reveal subtypes of this branch of the ligand-gated ion channel gene superfamily. Neuron *5*, 35–48.

Sine, S.M. (1997). Identification of equivalent residues in the gamma, delta, and epsilon subunits of the nicotinic receptor that contribute to alpha-bungarotoxin binding. J. Biol. Chem. *272*, 23521–23527.

Smit, A.B., Syed, N.I., Schaap, D., van Minnen, J., Klumperman, J., Kits, K.S., Lodder, H., van der Schors, R.C., van Elk, R., Sorgedrager, B., et al. (2001). A glia-derived acetylcholine-binding protein that modulates synaptic transmission. Nature *411*, 261–268.

Steinlein, O.K., Mulley, J.C., Propping, P., Wallace, R.H., Phillips, H.A., Sutherland, G.R., Scheffer, I.E., and Berkovic, S.F. (1995). A missense mutation in the neuronal nicotinic ACh receptor alpha 4 subunit is associated with autosomal dominant nocturnal frontal lobe epilepsy. Nat. Genet. *11*, 201–203.

Tsetlin, V. (1999). Snake venom alpha-neurotoxins and other 'three-finger' proteins. Eur. J. Biochem. *264*, 281–286.

Wang, H.L, Ohno, K., Milone, M., Brengman, J. Evoli, A., Batocchi, A.P., Middleton, L., Christodoulou, K., Engel, A.G., and Sine, S.M. (2000). Fundamental gating mechanism of nicotinic receptor channel gating revealed by mutation causing a congenital myasthenic syndrome. J. Gen. Physiol., *116*, 449–460.

Weiland, S., Witzemann, V., Villarroel, A., Propping, P., and Steinlein, O. (1996). An amino acid exchange in the second transmembrane segment of a neuronal nicotinic receptor causes partial epilepsy by altering its desensitization kinetics. FEBS Lett. *398*, 91–96.

Whiteaker, P., Sharples, C.G., and Wonnacott, S. (1998). Agonist-induced up-regulation of alpha4beta2 nicotinic acetylcholine receptors in M10 cells: pharmacological and spatial definition. Mol. Pharmacol. *53*, 950–962.

Zuo, J., De Jager, P.L., Takahashi, K.A., Jiang, W., Linden, D.J., and Heintz, N. (1997). Neurodegeneration in Lurcher mice caused by mutation in delta 2 glutamate receptor gene. Nature *388*, 769–773.

Zwart, R., and Vijverberg, H.P. (1998). Four pharmacologically distinct subtypes of alpha4beta2 nicotinic ACh receptor expressed in *Xenopus* laevis oocytes. Mol. Pharmacol. *54*, 1124–1131.